**Michigan Technological University**
Department of Mechanical Engineering – Engineering Mechanics

# Richard and Elizabeth Henes Professor of Computational Mechanics

# 2018 Annual Report

Gregory M. Odegard

September 15, 2017

## Introduction

The purpose of this report is to detail the research activities that were performed with support from the endowed position titled "Richard and Elizabeth Henes Professor of Computational Mechanics". This position has been held since 2014 by Prof. Gregory M. Odegard of the Department of Mechanical Engineering – Engineering Mechanics (MEEM) at Michigan Technological University. Prof. Odegard is the Associate Chair and Director of Graduate Studies in the department, The director of the NASA Space Technology Research Institute (STRI) for Ultra-Strong Composite Materials by Computational Design (US-COMP), and the Site Director for the NSF supported Industry/University Collaborative Research Center (I/UCRC) on Novel High Voltage/Temperature Materials and Structures (NVT).

Prof. Odegard would sincerely like to thank the Henes family for their generous gift. Their continuous support for the MEEM department has made a difference in raising our profile among ME department around the country and has played an important role in improving the educational experience of both undergraduate and graduate students in our department.

## Supported students

Between July 2017 and June 2018, the funds generated by this endowment were used to support PhD students Sorayot Chinkanjanarot ("Choi") and Hashim Al Mahmud. Choi was partially supported by a fellowship from the Thai government to study in the U.S. However, the amount of support that he received from the Thai government was not enough to cover his tuition and living expenses. Thus, some of the funds generated from the Richard and Elizabeth Henes Professor of Computational Mechanics endowment were used support Choi. The decision to support Choi in this manner was made because of Choi's dedication, hard work, and natural engineering talent; and the need to keep him as a PhD student at Michigan Tech. If we had not supported him in this manner, he most likely would have pursued a PhD student at another university, and we would have lost out on his talent.

Similarly, Hashim is partially supported by a fellowship from the Iraq government to study in the U.S. Some of the Henes funds have been used to augment his government support to keep him in our department. He is a very dedicated, hard-working student and is worthy of this support. Similar to Choi, I feel that we need to do what we can to keep Hashim as a PhD student in our department.

## Resulting research accomplishments

*Choi's research*

During the time period between June 2017 and December 2017, Choi conducted research on the molecular modeling of epoxy materials. This research is important

for the power transmission and aerospace industries, and is guided by the sponsors of our HVT center. Specifically, Boeing and CTC Global (manufacturer of new-generation power transmission cables) are interested in epoxy-based nanocomposites to improve the performance of composite structures and power transmission line durability, respectively. The material that Choi is specifically examining is known as a cyclo-aliphatic epoxy (CE) resin reinforced with graphite nanoparticles (GNPs). CE resins are known to be more durable and weather resistant than standard epoxy materials, and thus are more well-suited for the environmental conditions that airplane structures and power cables are typically subjected to. The addition of GNPs into the resin helps to raise the material strength, fracture toughness, and aging resistance.

Because of the difficulty in preparing test samples of these nanocomposites materials in terms of time, expense, and man-power; our research group specializes in computational simulation of materials for a more rapid and efficient exploration of material design space. That is, using well-developed computational tools (molecular dynamics, micromechanics, finite element analysis), we can predict the properties of materials based on material design parameters (e.g. GNP volume fraction, carbon fiber volume fraction, GNP dispersion) for a fraction of the cost of fabricating and testing different designs of these materials in the lab. Thus, these methods are ideal for the CE/GNP nanocomposites materials.

Choi's work was focused on developing computational methods to predict the thermal conductivity of these nanocomposites based on the material structure at the molecular level. By studying the molecular structure of the CE/GNP nanocomposite, and by manipulating this molecular structure, we can design a material with an optimal thermal conductivity. A higher thermal conductivity is important for dispersing the thermal energy of localized hot spots in the structure to partially mitigate the long-term effects of aging. For example, composite structures in aircraft suffer from localized heating near the tips of control surfaces and engine housing, whereas the composite structure in power transmission cables can suffer from localized heating near failing connections or areas exposed to intense sunlight. Higher thermal conductivities will disperse this heat into the rest of the structure, minimizing local energy hot spots and thus extending the life of the composite component.

Choi's work successfully established modeling methods to predict thermal conductivity, and his work on the CE/GNP nanocomposites matches very well with experiments, thus validating his modeling methods. As a result, we are getting closer to being able to fully design the CE/GNP nanocomposite with optimal properties for improved performance. Choi finished his PhD studies after the fall 2017 semester. With the support of the Henes funds, he was able to finish writing two journal articles and numerous conference papers. One of the journal articles has been published, and the other is currently under review. The published article is attached to this report.

*Hashim's research*

During the time period between July 2017 and June 2018, Hashim conducted research on the molecular simulation of epoxy/GNP composites. This work is focused on finding epoxy-based nanocomposite materials with improved mechanical properties (strength, stiffness) relative to traditional composites. This is important for aerospace applications in which lightweight material need to be used that are resistant to high loads. Hashim's work is a follow-on to the research of Cameron Hadden, a PhD student who graduated from our group a few years ago. Hashim is adding an important level of complexity to Cameron's results. Whereas Cameron only considered small mechanical deformations (elastic regime), Hashim's work is exploring the mechanical failure of these materials. This requires the use of a non-linear atomic potential, which is a mathematical relationship that describes the forces between atoms as a function of inter-atomic distance.

Hashim has successfully built computational models of the material and simulated the results. His work has shown that the nonlinear atomic potential (ReaxFF) works very well to predict the mechanical properties of these materials. He has shown this by comparison with our previous experiments on this material. In the future, these results will allow us to make more powerful and accurate predictions of material behavior for designing aerospace structures. Hashim gave a presentation at the 2018 ASCE (American Society of Civil Engineers) Earth and Space Conference in Cleveland, OH, April 2018. He has completed a manuscript of his first journal article. The article will be submitted by the end of this summer. It is anticipated that Hashim will complete a second manuscript within the next year.

Please don't hesitate to contact Prof. Odegard with any questions that you may have regarding this research or the use of the endowment funds. It is hoped that we can put this gift to use in the best possible way to facilitate our department's growth in research to be more globally competitive.

Journal of Applied Polymer Science

# Multiscale thermal modeling of cured cycloaliphatic epoxy/carbon fiber composites

Sorayot Chinkanjanarot, Matthew S. Radue, S. Gowtham, Julie M. Tomasi, Danielle R. Klimek-McDonald, Julia A. King, Gregory M. Odegard
Michigan Technological University, 1400 Townsend Drive, Houghton, Michigan 49931
Correspondence to: G. M. Odegard (E-mail: gmodegar@mtu.edu)

**ABSTRACT:** Cycloaliphatic epoxies (CEs) are commonly used for structural applications requiring improved resistance to elevated temperatures, UV radiation, and moisture relative to other epoxy materials. Accurate and efficient computational models can greatly facilitate the development of CE-based composite materials for applications such as Aluminum Conductor Composite Core high-voltage power lines. In this study, a new multiscale modeling method is developed for CE resins and composite materials to efficiently predict thermal properties (glass-transition temperature, thermal expansion coefficient, and thermal conductivity). The predictions are compared to experimental data, and the results indicate that the multiscale modeling method can accurately predict thermal properties for CE-based materials. For 85% crosslink densities, the predicted glass-transition temperature, thermal expansion coefficient, and thermal conductivity are 279°C, 109 ppm $°C^{-1}$, 0.24 W $m^{-1}$ $K^{-1}$, respectively. Thus, this multiscale modeling method can be used for the future development of improved CE composite materials for thermal applications. © 2018 Wiley Periodicals, Inc. J. Appl. Polym. Sci. 2018, *135*, 46371.

**KEYWORDS:** glass transition; resins; theory and modeling; thermal properties; thermosets

Received 15 November 2017; accepted 13 January 2018
**DOI: 10.1002/app.46371**

## INTRODUCTION

Cycloaliphatic epoxies (CEs) are commonly used for structural applications requiring improved resistance to elevated temperatures, UV radiation, and moisture relative to bisphenol A (DGEBA) and bisphenol F (DGEBF) diglycidyl ether epoxies.[1,2] Thus, CE composites are particularly important in applications such as high-voltage electrical insulators and Aluminum Conductor Composite Core (ACCC) high-voltage power transmission cables, particularly when they are paired with an anhydride curing agent (ACA) which also demonstrates remarkable environmental resistance. ACCC lines must withstand these harsh environmental conditions in addition to localized heating due to transmission line faults (i.e., failing connections and leakage currents). It is imperative that these lines be designed to mitigate localized heating quickly to reduce local material damage. Thus, the composite core component of the ACCC lines should have an optimal level of thermal conductivity. Also, the thermal expansion coefficient should be optimized to mitigate thermal sag in the lines. Accurate and efficient computational models can greatly facilitate the development of these composite core materials to meet these thermal property requirements.

Over the last decade, molecular dynamics (MD) simulation has become an important tool for the prediction of thermomechanical properties of epoxy materials. The thermal and mechanical response of DGEBF[3–13] and DGEBA[12,14–19] crosslinked epoxy systems has been investigated with numerous MD studies. These epoxy systems have become benchmark materials for MD simulation partially due to their relatively simple crosslinking reaction. For CE/ACA, the chain reaction mechanism is much more complex. The only known molecular modeling study for CE/ACA is from Komarov *et al.*,[20] who investigated the system using coarse-grained Monte Carlo simulation for crosslinking, followed by reversed-mapping to a fully atomistic MD model. Thus, a fully atomistic procedure for modeling the crosslinking of CE/ACA resins has not been developed.

The objectives of this study were to (1) develop an all-atom MD-based modeling procedure to accurately and efficiently simulate the crosslinking process of CE/ACA resins and to (2) predict the bulk-level thermal properties of carbon fiber-reinforced CE/ACA composites for a range of carbon fiber volume fractions using a multiscale modeling approach, which includes the MD modeling for atomic length scales and micromechanics for bulk length scales. The modeling procedure was validated with

Additional Supporting Information may be found in the online version of this article.

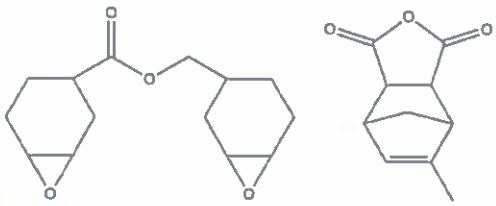

Figure 1. Molecular structure of EEC (left) and ACA (right).

experimental data determined as described herein and from the literature.

This article is structured as follows. First, the details of the polymer material system are provided, including the molecular structures of the resin and hardener and the curing mechanism. Second, details are provided about the multiscale modeling procedure. Third, the experimental methods for measurement of the mass density, glass-transition temperature, and thermal conductivity are described. Finally, the modeling results are discussed with respect to the experimental values.

## MATERIAL SYSTEM

Epoxy-cyclohexyl-methyl-3,4-epoxy-cyclohexyl-carboxylate (EEC) is a CE resin as characterized by the aliphatic carbon rings fused to reactive epoxide groups. For EEC, there are two epoxide groups per molecule as shown in Figure 1. The ACA is 4,7-methanoisobenzofuran-1,3-dione,3*a*,7,7*a*-tetrahydromethyl which contains a cyclic anhydride ring and bicyclic component, also shown in Figure 1.

The curing mechanism[21,22] of the EEC/ACA system consists of two main alternating reactions: an esterification reaction and a cyclic anhydride ring opening reaction. Figure 2 shows the esterification reaction between an epoxide group and carboxyl group, which requires a catalyst to start the reaction. This reaction generates an ester chain and hydroxyl group that is necessary for opening the cyclic anhydride ring. Figure 3 shows the cyclic anhydride ring opening reaction. This reaction is initiated by a hydroxyl group from the esterification reaction. A carboxyl group is created and continues again as the reactive group in the esterification reaction. Both reactions continue until all nearby reactive groups are reacted. The experimental curing condition[1] starts at 100 °C for 1 h, then heats up to 200 °C and held for 2 h. This is followed by a cool-down ramp to room temperature.

## MULTISCALE MODELING

The multiscale computational approach employed in this study includes both MD and micromechanical modeling, which cover different characteristic length scales. MD modeling was used to determine thermal properties of the neat epoxy based on the molecular structure. For the micromechanics modeling, the results from the MD modeling were used as input into a larger scale representative volume element (RVE) to predict the effective thermal conductivity of bulk-level carbon fiber/CE composites. All details of the modeling are given in this section.

### MD Modeling

All neat epoxy models were simulated at the molecular level using the large-scale atomic/molecular massively parallel simulator (LAMMPS) MD software package[23] with the optimized potentials for liquid simulations-all atom (OPLS-AA) force field.[24,25] Monomeric structures of EEC and ACA were initially created using ChemBioDraw[26] and subsequently imported into LAMMPS. The force constants associated with bond, angle, dihedral, and van der Waal (vdW) interactions were used. The topology of both monomers was equilibrated using the conjugated-gradient method, as implemented in LAMMPS, with a $1 \times 10^{-4}$ energy tolerance. MD simulations were subsequently performed with the NVT ensemble for 1 ns with 1 fs time steps. In Figure 4, the resulting molecular structures of EEC and ACA monomers were rendered using the Open Visualization Tool (OVITO) software package.[27]

For the simulated crosslinking, the curing mechanism discussed above required a catalyst to start the chain reaction. A subset of the ACA molecules were modified with an ethanol molecule,[28] as shown in Figure 5. The cyclic anhydride ring on the ACA molecule was opened with the hydroxyl group on the ethanol

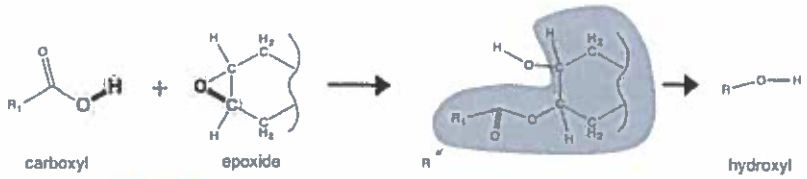


Figure 2. Esterification reaction between carboxyl and epoxide groups.


Figure 3. Cyclic anhydride ring opening reaction between hydroxyl group and anhydride ring.

Figure 4. Molecular models of EEC (left) and ACA (right). Red, oxygen; black, carbon; white, hydrogen. [Color figure can be viewed at wileyonlinelibrary.com]

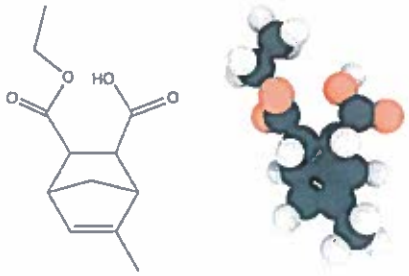


Figure 5. Molecular structure and molecular model of modified ACA. Red, oxygen; black, carbon; white, hydrogen. [Color figure can be viewed at wileyonlinelibrary.com]

molecule. The exposed carboxyl group was therefore available to react with epoxide groups for the esterification reaction (Figure 2).

Bulk molecular models of the EEC/ACA system were generated using a multistep process. The molar ratio between the CE resin and ACA was 1:2. The monomers of EEC, ACA, and modified ACA were mixed as shown in Table I. These monomers were combined in a large MD simulation box. The initial mass density of the simulation box was less than 0.008 g $cm^{-3}$ and all boundaries were periodic. For the results discussed herein, all thermal properties were determined from a cubic simulation box, except for the thermal conductivity simulations with direct method (described below), which utilized a prism-shaped simulation box.

Table I. The Number of Molecules and Atoms of Cubic and Prism Simulation Boxes

| | Number of molecules | | | Number |
|---|---|---|---|---|
| Shape | EEC | ACA | Modified ACA | of atoms |
| Cube | 84 | 156 | 12 | 7,164 |
| Prism | 126 | 234 | 18 | 10,746 |

The simulation boxes were alternately subjected to potential energy equilibrations and simulation box size reductions using the "minimize" and "fix deform" commands in LAMMPS, respectively. The simulation boxes were gradually compressed to a density of 1.2 g $cm^{-3}$, which is the accepted bulk density of most epoxy resins.[29] The box lengths in along the $x$, $y$, and $z$ directions were sequentially reduced to their final length by densifying in four different steps as shown in Table II over a total simulation time of 4.2 ns with 1 fs time steps. The density profiles of the densified models were spatially uniform along the $x$, $y$, and $z$ directions, and thus the MD models were well equilibrated in the uncrosslinked state.

The crosslinking process combined LAMMPS simulations and Python scripting in an iterative manner. All details are included in the Supporting Information. Crosslink densities of 60%, 65%, 70%, 75%, 80%, 85%, and 90% were chosen, where the crosslink density is defined as the percentage of all epoxy reactive groups that are crosslinked. For each crosslink density, a total of five independent models were established for accurate statistical sampling.

After the crosslinking process, the models were equilibrated with the NPT ensemble at 1 ATM and 300 K to allow residual stresses to be minimized. Figure 6 shows representative mass density profiles along each of the Cartesian axes. The relatively small fluctuations in density indicate that the model has minimal localized residual stresses within the simulation box. The mass density was calculated from averaging the last 10 ps of each simulation. The average mass densities and conversion levels are provided in Table III. Figure 7 shows a representative crosslinked model after equilibrating for 2 ns with 1 fs time steps. All structural details (bond length, angle, and dihedral angle) of equilibrated models are given in Supporting Information. After crosslinking, the models were ready for further simulation to predict the thermal properties.

**Glass-Transition Temperature.** The glass-transition temperature was determined for each crosslink density using the method of Bandyopadhyay *et al.*[6] The temperature of the crosslinked cubic EEC/ACA simulation boxes was increased from −100 to 527 °C (173–800 K) in the NPT ensemble under 1 atm pressure. The

Table II. The Length of the Cubic and Prism-Shape Simulation Boxes during the Densification

| | Cube (Å) | | | Prism (Å) | | | |
|---|---|---|---|---|---|---|---|
| Step | x | y | z | x | y | z | Time (ns) |
| 0 | 300.00 | 200.00 | 200.00 | 300.00 | 300.00 | 300.00 | — |
| 1 | 41.50 | 41.50 | 41.50 | 26.15 | 26.15 | 156.88 | 0.2 |
| 2 | 23.86 | 23.86 | 23.86 | 15.03 | 15.03 | 90.20 | 1.0 |
| 3 | 21.79 | 21.79 | 21.79 | 13.73 | 13.73 | 82.36 | 2.0 |
| 4 | 20.75 | 20.75 | 20.75 | 13.07 | 13.07 | 78.44 | 1.0 |

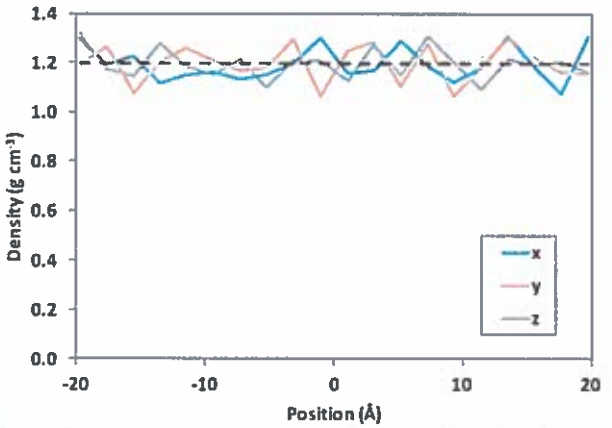


**Figure 6.** Density profiles of a 80% crosslinked cubic EEC/ACA model along *x*, *y*, and *z* axes. [Color figure can be viewed at wileyonlinelibrary.com]

model was gradually heated over 5 ns with 1 fs time steps. The heating rate was $1.25 \times 10^{11}$ °C $s^{-1}$. The mass densities and temperatures of the MD models were averaged every 2 ps throughout the simulations and plotted as shown in Figure 8 for a representative system. The two linear trend lines were fit using the "segmented" package[30] in the RStudio[31] integrated development environment. The glass-transition temperature was defined as the temperature corresponding to the interception of the trend lines. It is important to note that the simulated heating rate is orders of magnitude higher than those observed in laboratory environments. Given modern limitations in computational resources, laboratory heating rates cannot be efficiently simulated with MD. The effect of heating rate is discussed and quantified in the Results and Discussion section.

**Coefficient of Linear Thermal Expansion.** The coefficient of linear thermal expansion (CLTE) was determined using the same output from the heating-up simulations for the glass-transition temperature. Specifically, the CLTE was calculated from

$$\alpha = \frac{\beta}{3} = \frac{1}{3}\left(\frac{1}{V}\frac{\partial V}{\partial T}\right) \quad (1)$$

where β is the coefficient of volumetric thermal expansion (CVTE). For each simulation, the system temperatures and volumes were averaged every 2 ps. Figure 9 shows a representative plot between volume and temperature. A polynomial function of volume, $V(T)$, was fit to the data and differentiated with respect to the temperature ($T$) for eq. (1). In this study, the CLTE was calculated at 300 K (27 °C) for each of the crosslinking levels.

**Thermal Conductivity.** The thermal conductivities of the crosslinked models were determined by two different methods. The first method was the nonequilibrium MD (NEMD) approach, also known as the direct method based on Fourier's law. The second method was the equilibrium MD (EMD) approach based on the fluctuation–dissipation theorem, also known as the Green–Kubo[32] formalism. Both methods have been previously used to predict the thermal conductivities of Si[33] and EPON862 epoxy.[5]

The NEMD method requires a steady-state condition, and the thermal conductivity[34] is calculated using

$$\kappa = -\frac{J}{dT/dz} \quad (2)$$

where $J$ is the heat flux (rate of heat flow per unit area) and $dT/dz$ is the temperature gradient along the $z$-direction. A prism-shaped MD simulation box was used to predict the thermal gradient. Figure 10 shows a representative system with an aspect ratio of 6 which this configuration was developed by Varshney *et al.*[35] The prism model was divided into 20 equally sized slabs along the length. The positions of the atoms in the slabs on both ends of the simulation box were fixed. The temperatures of the slabs next to the end slabs were held at 250 and 350 K (red and blue slabs in Figure 11, respectively) using the NVT ensemble with 5 fs of temperature damping to obtain an overall temperature of 300 K. The energies of the middle slabs were conserved with the NVE ensemble. The heat flux was calculated using

$$J = \frac{(Q_{hot} - Q_{cold})/2}{At} \quad (3)$$

The total heat ($Q_{hot} - Q_{cold}$) was divided by 2 because the heat was transferred to both sides of the simulation box. The NEMD simulation ran for 4 ns with 1 fs time steps. The first 2 ns of the simulation established the temperature gradient into a steady-state condition. The final 2 ns of the simulation was used to determine the average temperature in each slab, as

**Table III.** The Crosslink Densities and Mass Densities of MD Models

| Cube | | Prism | |
|---|---|---|---|
| Crosslink density | Mass density (g $cm^{-3}$) | Crosslink density | Mass density (g $cm^{-3}$) |
| 0.60 ± 0.00 | 1.211 ± 0.003 | 0.60 ± 0.00 | 1.209 ± 0.005 |
| 0.66 ± 0.01 | 1.214 ± 0.006 | 0.65 ± 0.00 | 1.206 ± 0.004 |
| 0.70 ± 0.00 | 1.210 ± 0.004 | 0.70 ± 0.00 | 1.207 ± 0.005 |
| 0.75 ± 0.01 | 1.204 ± 0.004 | 0.75 ± 0.00 | 1.204 ± 0.005 |
| 0.80 ± 0.00 | 1.199 ± 0.006 | 0.80 ± 0.00 | 1.193 ± 0.005 |
| 0.85 ± 0.00 | 1.191 ± 0.006 | 0.85 ± 0.00 | 1.187 ± 0.005 |
| 0.90 ± 0.00 | 1.183 ± 0.007 | 0.90 ± 0.01 | 1.187 ± 0.001 |

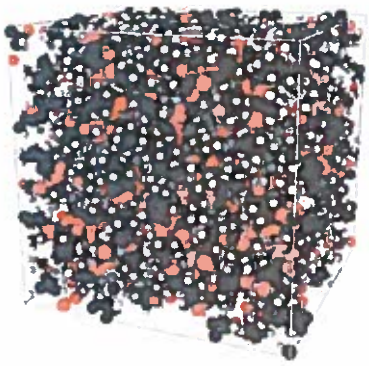

Figure 7. Representative crosslinked cubic model of EEC/ACA after equilibration. [Color figure can be viewed at wileyonlinelibrary.com]

shown in Figure 12. Also included in the figure are the inlet and outlet temperatures for calculating the thermal conductivity using eq. (2).

For the EMD method, the thermal conductivity[36] in the $x$ direction is calculated using

$$\kappa_x = \frac{V}{k_B T^2}\int_0^{\infty} \langle J_x(0)J_x(t)\rangle dt \tag{4}$$

where $V$ is the system volume, $k_B$ is the Boltzmann constant, $T$ is the system temperature, and $\langle J_x(0)J_x(t)\rangle$ is the heat current autocorrelation function (HCACF). The EMD method can determine the thermal conductivity of an isotropic material by averaging the properties along the $x$, $y$, and $z$ axes using

$$\kappa = \frac{V}{3k_B T^2}\int_0^{t} \langle \mathbf{J}(0)\cdot\mathbf{J}(t)\rangle dt \tag{5}$$

where the heat flux vector is

$$J = \frac{1}{V}\left[\sum_i E_i \mathbf{v}_i - \sum_i \mathbf{S}_i \mathbf{v}_i\right] \tag{6}$$

and

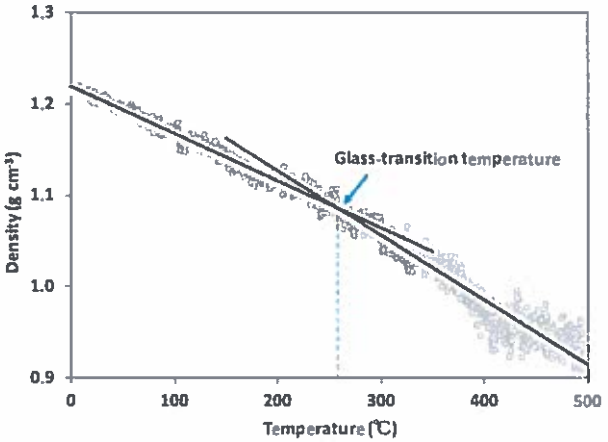


Figure 8. Plot of mass density versus temperature for determining glass-transition temperature for a EEC/ACA model of 80% crosslink density. [Color figure can be viewed at wileyonlinelibrary.com]

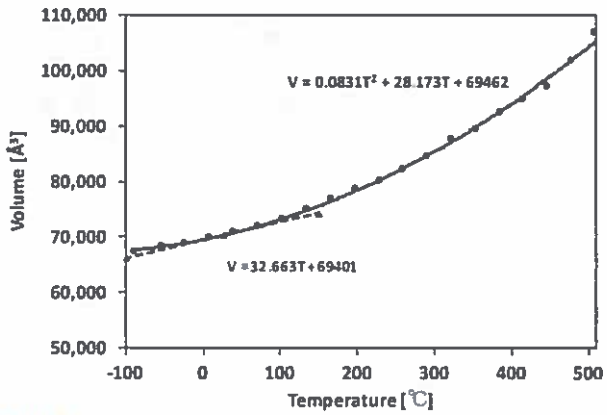


Figure 9. Plot of simulation box volume as a polynomial function of temperature from a representative 80% crosslinked cubic model with the polynomial trend line (solid line) and tangent line (dashed line) at 27 °C.

$$E_i = \frac{1}{2} m_i \mathbf{v}_i^2 + \frac{1}{2} U_i \tag{7}$$

where the first term is the total kinetic energy; $\mathbf{v}_i$ and $m_i$ are the velocity vector and mass of atom $i$, respectively; and $U_i$ is the total potential energy of atom $i$ which includes the 12–6 Lennard–Jones potential for van der Waals interactions. The bonded interactions include the stretching (bond), bending (angle), and torsional (dihedral) energies. $\mathbf{S}_i$ in eq. (6) is the per-atom stress tensor of atom $i$.

Cubic MD simulation boxes were used to determine thermal conductivities via the EMD method by initially maintaining the temperature at 300 K with the NVT ensemble. The simulations ran for 10 ps with 1 fs time steps with a 10 Å Lennard–Jones cutoff. The "compute heat/flux" command in LAMMPS was subsequently utilized to compute the heat flux from the potential energy, kinetic energy, and stress values. The HCACF was obtained by using the autocorrelation average with the "fix ave/correlate" command in LAMMPS.

The integral term in eq. (5) was calculated using the trapezoidal rule for 50 ps of the correlation time ($t_c$) with 5 fs time increments. The fluctuation of the HCACF decayed to zero after 4 ps, as shown in Figure 13. The data in the figure suggests that the correlation time ($t_c = 50$ ps) is sufficiently large for this system, as the results stabilized at a much smaller timeframe (~1 ps). The thermal conductivity of the EEC/ACA system was calculated from eq. (5) and is shown in Figure 13. The thermal conductivity was averaged from the final 10 ps of the autocorrelation time. The value of 10 ps was chosen since it is sufficiently large enough to sample the fluctuations in the thermal conductivity, as shown in Figure 13.

### Micromechanics

The bulk thermal conductivity of the unidirectional carbon fiber/CE composite was predicted using micromechanics calculations. Specifically, the thermal conductivities of the epoxy matrix were taken from the MD simulations described above and the AS4 carbon fiber properties were taken from the literature[37] (axial thermal conductivity = 6.5 W $m^{-1}$ $K^{-1}$ and

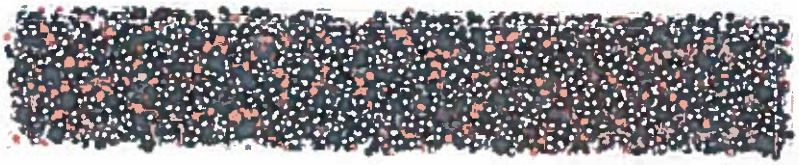

Figure 10. A representative prism-shaped model for determining the thermal conductivity using NEMD. [Color figure can be viewed at wileyonlinelibrary.com]

transverse thermal conductivity = 2.18 W $m^{-1}$ $K^{-1}$). The uncertainties in the thermal conductivities for the neat epoxy represent the standard deviation from the multiple MD predictions. Three different values of the properties of the neat epoxy were used in the micromechanics predictions: the mean value and the mean value ± one standard deviation. This provided the uncertainty in the properties at the bulk level based on the uncertainty at the molecular level.

The micromechanics analysis code based on the generalized method of cells (MAC/GMC)[38] was used for the micromechanics predictions. A circular fiber approximation (rectangular pack or "Architecture 13" as implemented in MAC/GMC) was used as a repeating unit cell (RUC). This RUC has 26 × 26 subcells in which 312 middle subcells represented the fiber region and the other subcells represented the matrix region. The calculation of the effective thermal conductivities of the carbon fiber/CE composite included fiber volume fractions ranging from 5% to 80% with 5% increments.

## EXPERIMENTAL

### Fabrication of Neat TTA21L (CE) Epoxy

The EEC/ACA neat epoxy was fabricated using a FlackTek SpeedMixer DAC 150.1 FVZ by pouring resin and hardener in a 100 g:138 g ratio into five mixing cups of 90 g each, for a total batch size of 450 g. Each cup was mixed in the SpeedMixer for 2 min at 2500 rpm. The cups were degassed at 100 °C and 29 in Hg vacuum until no more bubbles appeared. The mixture was then poured into a preheated mold and degassed again under full vacuum. The mold was coated with Mann Ease Release 300. The preheating and final degassing were performed at 100 °C. The curing cycle was 100 °C for 1 h, then heated to 200 °C at 2 °C $min^{-1}$, then held at 200 °C for 2 h. The oven was turned off and the cured epoxy was allowed to cool in the oven to room temperature at a ~1 °C $min^{-1}$ cooling rate. The molds made about 20 rectangular bars (165 mm long by 19 mm wide by 3.3 mm thick) and 5 disks (64 mm diameter and 3.2 mm thick), from which the testing specimens were machined. The density of the samples was measured at 23 °C according to ASTM D792.[39]

Figure 11. Simulation box including fixed slabs (gray), 350 K slab (red), 250 K slab (blue), and middle slabs (white). [Color figure can be viewed at wileyonlinelibrary.com]

### Dynamic Mechanical Analysis Testing for Glass-Transition Temperature

Dynamic mechanical analysis (DMA) was used to find the glass-transition temperature of the epoxy samples. The tests were conducted with a TA Instruments Q800 DMA using the dual/single cantilever clamp. The single cantilever geometry was used for all testing, with a set length of 17.5 mm between clamps. The sample dimensions were 3.3 mm thick, 12 mm wide, and 35 mm long; and were cut from the rectangular bars. Samples were rinsed with isopropyl alcohol before testing. Each sample was loaded into the clamps and tightened down using 8 in-lb of torque. Tweezers were used to keep the sample surfaces free of oil from hands and fingers.

Once the samples were in placed in the clamps, amplitude sweep tests were performed. The test mode was set to "DMA Multi Strain" with the test set to "Strain Sweep." The frequency was kept at 1 Hz with the isothermal temperature at 35 °C and a soak time of 5 min. The amplitude was swept from 5 to 50 μm. Following these tests, graphs of amplitude versus loss modulus were analyzed to determine the amplitude needed for the temperature sweep test.

### Thermal Conductivity Testing

Through-plane thermal conductivity was measured using a Holometrix Model TCA-300 Thermal Conductivity Analyzer, which follows the ASTM F433[40] guarded heat flow meter method. The though-plane thermal conductivities of the 3.2 mm thick, 50 mm diameter disc-shaped test specimens were measured at 55 °C.

## RESULTS AND DISCUSSION

The average mass densities of the cubic and prism models at each crosslink density are shown in Table III. The mass density

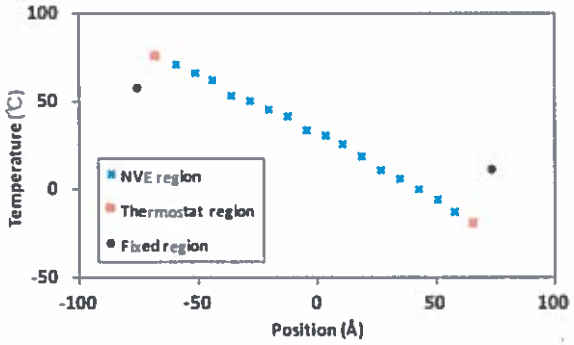


Figure 12. Representative temperature gradient along simulation box. [Color figure can be viewed at wileyonlinelibrary.com]

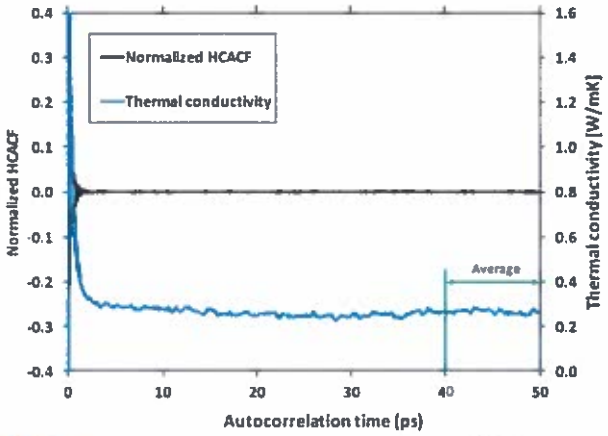


**Figure 13.** Representative plot of the normalized HCACF and thermal conductivity of the CE system as a function of autocorrelation time ($t_c$). [Color figure can be viewed at wileyonlinelibrary.com]

values are in good agreement with the experimentally obtained value of $1.219 \pm 0.001$ g cm$^{-3}$. In general, the predicted mass densities of both cubic and prism MD models decreased with increased crosslink density. The mass density reduction is likely a result of the decrease in chain flexibility with increases in crosslink density. At lower crosslink densities, the monomers can be positioned closer together with little constraint. At higher crosslink densities, the additional covalent bonds between monomers increase constraining forces, thus prohibiting full structural densification.

Figure 14 shows the glass-transition temperature averaged over five different models for each crosslink density with their standard deviations as the error bars. With five independent models per each crosslink density, the results are statistically significantly different ($F = 16.7$ and $F_{crit} = 2.4$ from ANOVA test). The plot shows that the glass-transition temperature is crosslink density dependent, as was previously observed with the EPON862 system.[6] The experimental glass-transition temperature (dashed line) was $250.58 \pm 1.05$ °C. The experimental heating rate is about 12 orders of magnitude lower than the simulated heating rate (due to computational limitations associated with MD simulation). Due to the heating rate effect, the glass-transition temperature increases 3 °C when the heating rate increases by an order of magnitude.[7,41] The adjusted glass-transition temperature (solid line) is corrected by adding 36 °C to the experimental (original) value. The predicted glass-transition temperatures for 85% and 90% crosslink densities are in good agreement with the experiment, for which the crosslink density is not known precisely, but are typically in the range of 90% for most epoxies.

Figure 15 shows the predicted CLTE of the epoxy as a function of crosslink density at 300 K. A range of experimental CLTE values from the literature[12–16] (with unknown crosslink density) are included in the plot. The plot demonstrates that the predicted CLTE decreases with increasing crosslink density. A similar trend for the CLTE of a CE system was observed by Komarov *et al.*[20] From the figure it is also evident that the predicted CLTE values approach the experimental values at increasing levels of crosslink density. Because most epoxies are expected to have relatively high crosslink densities, there is satisfactory agreement between models and literature values. Also, the closest agreement with experiment in the figure corresponds with the 85% and 90% crosslink density level range, which agrees with the glass-transition temperature data shown in Figure 14, indicating that the experimental crosslink density is likely in this same range (crosslink densities are typically around 90% for most epoxies). It is important to note that the modeling simulates a highly packed amorphous system, whereas experimental specimens may contain small volume fractions of voids or gasses, which would effectively lower the CLTE. This may help explain some of the discrepancy shown in Figure 15, however, this cannot be stated conclusively since an in-depth multiscale modeling study on the effects of voids on bulk-scale properties has not be conducted, to the authors' knowledge.

The decrease in CLTE with increasing crosslink densities can be explained by the overall increase in covalent bonds and the thus the decreasing influence of weaker van der Waals forces on the internal structural rigidity of the system. As a result, molecular

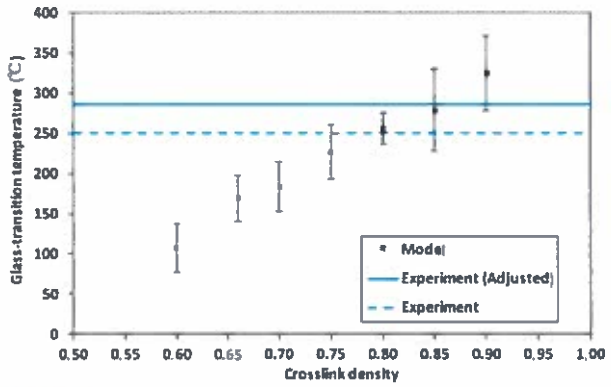


**Figure 14.** Predicted glass-transition temperatures of cured epoxy models as a function of crosslink density. Experimentally obtained value (with unknown crosslink density) is overlaid on the data. [Color figure can be viewed at wileyonlinelibrary.com]

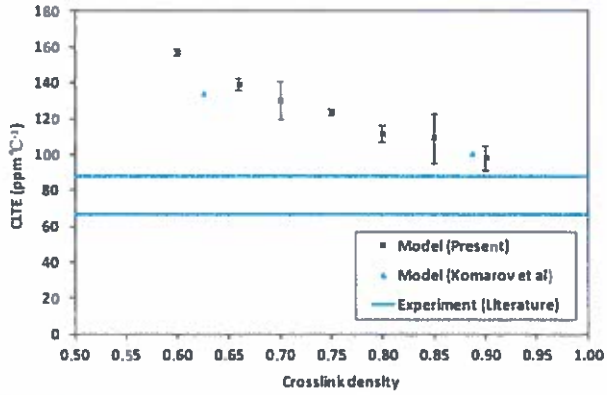


**Figure 15.** Plot of predicted CLTE as a function of crosslink density at 300 K. Literature (experiment) values of unknown crosslink density are overlaid and predicted values from literature are also included. [Color figure can be viewed at wileyonlinelibrary.com]

mobility is reduced, and the interaction of adjacent molecular groups is increased with increases in crosslink density. Thus, increases in temperature will have a reduced influence on the material density. As a result, the CLTE drops. As the CLTE and molecular mobility drop with increasing crosslink density, the glass-transition temperature is forced to shift to higher temperatures. That is, higher temperatures and thermal energies are necessary to reduce the structural rigidity of the system.

Figure 16 provides the predicted average thermal conductivities of the CE epoxy system averaged over the five models using the EMD and NEMD methods. The error bars represent the standard deviations associated with the five models at each crosslink density. It is important to note that the error bars for the EMD method are larger than those of the NEMD method because of inherent computational difficulties associated with the EMD method.[47] Given the uncertainty levels, the results suggest that the two methods are in general agreement. This behavior is similar to that observed with MD modeling of the EPON862 system.[5] The thermal conductivity from NEMD is dependent on the crosslink density but the EMD cannot capture the crosslinking dependence. The results also suggest that the predicted thermal conductivities are within the range of the experimental thermal conductivity values reported in the literature.[48-54] However, the predicted thermal conductivities are significantly higher than those from the experiment described herein. The experiments were repeated under identical conditions, which are consistent with the methods discussed in the literature. The source of the discrepancy is uncertain; however, it is clear that the agreement with the literature values serves as a validation of the simulation techniques. Again, it is important to note that trapped voids/gasses in experimentally prepared specimens could potentially explain some of the discrepancy, since these are not included in the perfectly packed simulated amorphous structures. However, the extent of this influence on the bulk properties is not known (from the modeling perspective), to the authors' knowledge.

Figure 17 shows the predicted thermal conductivities of a unidirectional EEC/ACA/carbon fiber composite parallel ($k_{11}$) and transverse ($k_{22} = k_{33}$) to the fiber direction. The effective axial and transverse thermal conductivities increase linearly and nonlinearly, respectively, with the carbon fiber volume fraction. The standard deviations of these calculations are relatively small and the corresponding error bars are partially hidden by the data points in Figure 17. The predicted thermal conductivities are in good agreement with experimental values from the literature,[55-58] thus further validating the multiscale computational modeling method.

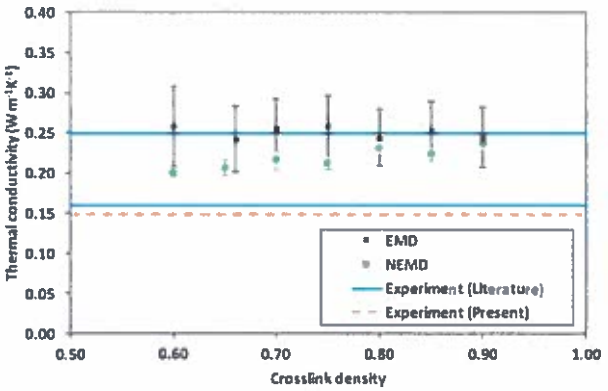


**Figure 16.** Plot of predicted NEMD and EMD thermal conductivities as a function of crosslink density. Literature and experimentally obtained values of unknown crosslink density are overlaid on the data. [Color figure can be viewed at wileyonlinelibrary.com]

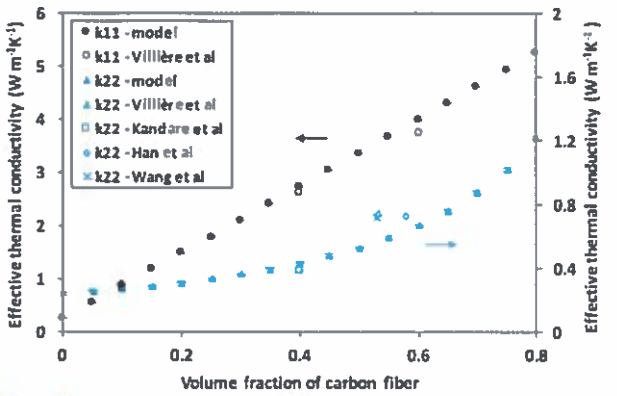


**Figure 17.** Plot of thermal conductivity as a function of carbon fiber volume fraction parallel (circle) and transverse (triangle) to the fiber direction. Experimental values taken from literatures.[55–58] [Color figure can be viewed at wileyonlinelibrary.com]

## CONCLUSIONS

There are two important results from this research. First, an all-atom MD modeling method for CE epoxies was developed and validated with comparison to experimental data for glass-transition temperature, CLTE, and thermal conductivity. To the best of the authors' knowledge, this is the first such method developed specifically for CE resins. Second, the multiscale modeling approach developed in this study, which uses results of MD and micromechanical modeling, can accurately predict the bulk-level thermal conductivity of CE-based composite materials. The multiscale approach was validated with comparison of predicted thermal conductivity values of CE/carbon fiber composites to those found in the literature.

The developed multiscale modeling method can be used to facilitate the development of CE-based epoxy composites and nanocomposite materials for thermal applications. By taking advantage of low-cost simulations to establish preliminary material designs, overall materials development costs can be dramatically reduced and development times can be expedited. This ability to efficiently develop new CE-based composite materials is particularly important for the continued development of ACCC high-transmission power lines. It is also possible to use this approach for a wide range of other polymer composite systems, although in-depth studies need to be performed.

## ACKNOWLEDGMENTS

This research was funded by the NSF I/UCRC on Novel High Voltage/Temperature Materials and Structures (grant IIP-1362040)

and the Richard and Elizabeth Henes Endowment at Michigan Tech. SUPERIOR and ATHENA, high-performance computing clusters at Michigan Technological University, were used in obtaining results presented in this publication.

## REFERENCES


1. Tomasi, J. M.; Helman, I. D.; Pisani, W. A.; Klimek-McDonald, D. R.; Chinkanjanarot, S.; Miskioglu, I.; King, J. A.; Odegard, G. M. *Polym. Degrad. Stab.* **2016**, *133*, 131.
2. Middleton, J.; Burks, B.; Wells, T.; Setters, A. M.; Jasiuk, I.; Kumosa, M. *Polym. Degrad. Stab.* **2013**, *98*, 2282.
3. Fan, H. B.; Yuen, M. M. F. *Polymer* **2007**, *48*, 2174.
4. Varshney, V.; Patnaik, S. S.; Roy, A. K.; Farmer, B. L. *Macromolecules* **2008**, *41*, 6837.
5. Varshney, V.; Patnaik, S. S.; Roy, A. K.; Farmer, B. L. *Polymer* **2009**, *50*, 3378.
6. Bandyopadhyay, A.; Valavala, P. K.; Clancy, T. C.; Wise, K. E.; Odegard, G. M. *Polymer* **2011**, *52*, 2445.
7. Li, C. Y.; Strachan, A. *Polymer* **2011**, *52*, 2920.
8. Bandyopadhyay, A.; Odegard, G. M. *Model. Simul. Mater. Sci. Eng.* **2012**, *20*, 045018.
9. Hadden, C. M.; Jensen, B. D.; Bandyopadhyay, A.; Odegard, G. M.; Koo, A.; Liang, R. *Compos. Sci. Technol.* **2013**, *76*, 92.
10. Kravchenko, O. G.; Li, C.; Strachan, A.; Kravchenko, S. G.; Pipes, R. B. *Compos. Part A: Appl. Sci. Manuf.* **2014**, *66*, 35.
11. Odegard, G. M.; Jensen, B. D.; Gowtham, S.; Wu, J.; He, J.; Zhang, Z. *Chem. Phys. Lett.* **2014**, *591*, 175.
12. Li, C. Y.; Strachan, A. *J. Polym. Sci. Part B: Poly. Phys.* **2015**, *53*, 103.
13. Radue, M. S.; Jensen, B. D.; Gowtham, S.; Klimek-McDonald, D. R.; King, J. A.; Odegard, G. M. *J. Polym. Sci. Part B: Polym. Phys.* **2018**, *56*, 255.
14. Wu, C. F.; Xu, W. J. *Polymer* **2006**, *47*, 6004.
15. Fan, H. B.; Chan, E. K. L.; Wong, C. K. Y.; Yuen, M. M. F. *J. Electron. Packag.* **2007**, *129*, 35.
16. Shenogina, N. B.; Tsige, M.; Patnaik, S. S.; Mukhopadhyay, S. M. *Macromolecules* **2012**, *45*, 5307.
17. Soni, N. J.; Lin, P. H.; Khare, R. *Polymer* **2012**, *53*, 1015.
18. Kumar, A.; Sundararaghavan, V.; Browning, A. R. *Model. Simul. Mater. Sci. Eng.* **2014**, *22*, 025013.
19. Hamerton, I.; Tang, W.; Anguita, J. V.; Silva, S. R. P. *React. Funct. Polym.* **2014**, *74*, 1.
20. Komarov, P. V.; Yu-Tsung, C.; Shih-Ming, C.; Khalatur, P. G.; Reineker, P. *Macromolecules* **2007**, *40*, 8104.
21. Stevens, G. C. *J. Appl. Polym. Sci.* **1981**, *26*, 4259.
22. Park, S.-J.; Kwak, G.-H.; Sumita, M.; Lee, J.-R. *Polym. Eng. Sci.* **2000**, *40*, 2569.
23. Plimpton, S. *J. Comput. Phys.* **1995**, *117*, 1.
24. Jorgensen, W. L.; Maxwell, D. S.; Tirado-Rives, J. *J. Am. Chem. Soc.* **1996**, *118*, 11225.
25. Jorgensen, W. L. OPLS All-Atom Parameters for Organic Molecules, Ions, Peptides & Nucleic Acids. **2008**.
26. CambridgeSoft. ChemDraw; PerkinElmer, Inc.: Waltham, MA, **2015**.
27. Stukowski, A. *Model. Simul. Mater. Sci. Eng.* **2010**, *18*, 015012.
28. Zhang, M.; Huang, Z. X.; Qin, Y. *Adv. Mater. Res.* **2009**, *79–82*, 1193.
29. SC:1183-02/EPIKOTE™ Resin 862/EPIKURE™ Curing Agent W System. Resolution Performance Products LLC.
30. Muggeo, V. M. R. *Stat. Med.* **2003**, *22*, 3055.
31. Team, R. RStudio: Integrated Development; R. RStudio, Inc.: Boston, MA, **2015**.
32. Kubo, R.; Toda, M.; Hashitsume, N. Statistical Physics II Nonequilibrium Statistical Mechanics; Springer-Verlag: Berlin, Germany, **1991**.
33. Schelling, P. K.; Phillpot, S. R.; Keblinski, P. *Phys. Rev. B* **2002**, *65*, 144306.
34. Anderson, C. V. D. R.; Tamma, K. K. *Int. J. Numer. Methods Heat Fluid Flow* **2004**, *14*, 12.
35. Varshney, V.; Roy, A. K.; Baur, J. Presented at the Twenty-Ninth Technical Conference on Composite Materials. Price Center, University of California San Diego, La Jolla, CA, **2014**.
36. Evans, D. J.; Morriss, G. P. Statistical Cechanics of Nonequilibrium Liquids, 2nd ed.; Cambridge University Press: New York, NY, **2008**.
37. Jordan, A.; Whetsell, J. L.; Mrinal, C.; Saha, M.; Altan, C. Presented at the 29th Annual American Society of Composite, San Diego, CA, September **2014**.
38. Brett, B.; Arnold, S. M. MAC/GMC User's Manual—Keywords Manual; NASA Center for Aerospace Information: Hanover, MD, **2002**; Vol. *2*.
39. ASTM D792-13, Standard Test Methods for Density and Specific Gravity (Relative Density) of Plastics by Displacement; West Conshohocken, PA, **2013**.
40. ASTM F433-02(2014)e1, Standard Practice for Evaluating Thermal Conductivity of Gasket Materials; West Conshohocken, PA, **2014**.
41. Ferry, J. D. Viscoelastic Properties of Polymers; John Wiley: New York, NY, **1980**.
42. Chen, Z.; Liu, Z.; Shen, G.; Wen, R.; Lv, J.; Huo, J.; Yu, Y. *Ind. Eng. Chem. Res.* **2016**, *55*, 7635.
43. Zhao, L. N.; Zhang, L.; Wang, Z. G. *RSC Adv.* **2015**, *5*, 95126.
44. Liu, W.; Wang, Z.; Chen, Z.; Li, J.; Zhao, L. *Polym. Adv. Technol.* **2012**, *23*, 367.
45. Xie, M. R.; Wang, Z. G. *Macromol. Rapid Commun.* **2001**, *22*, 620.
46. Wong, C. P.; Bollampally, R. S. *J. Appl. Polym. Sci.* **1999**, *74*, 3396.
47. Zhang, Y.; Otani, A.; Maginn, E. J. *J. Chem. Theory Comput.* **2015**, *11*, 3537.
48. Fang, L.; Wu, C.; Qian, R.; Xie, L.; Yang, K.; Jiang, P. *RSC Adv.* **2014**, *4*, 21010.
49. Gao, J.; Yu, J.; Wu, X.; Rao, B.; Song, L.; He, Z.; Lu, S. *Fibers Polym.* **2015**, *16*, 2617.
50. Peng, W.; Huang, X.; Yu, J.; Jiang, P.; Liu, W. *Compos. Part A: Appl. Sci. Manuf.* **2010**, *41*, 1201.
51. Yan, H.; Wang, R.; Li, Y.; Long, W. *J. Electron. Mater.* **2015**, *44*, 658.

52. Yu, J. H.; Duan, J. K.; Peng, W. Y.; Wang, L. C.; Peng, P.; Jiang, P. K. *Express Polym. Lett.* **2011**, *5*, 132.

53. Yu, J.; Huang, X.; Wu, C.; Wu, X.; Wang, G.; Jiang, P. *Polymer* **2012**, *53*, 471.

54. Zhong, H S.; Rubinsztajn, Organic Matrices Containing Nanomaterials to Enhance Bulk Thermal Conductivity, Google Patents. **2006**.

55. Villière, M.; Lecointe, D.; Sobotka, V.; Boyard, N.; Delaunay, D. *Compos. Part A: Appl. Sci. Manuf.* **2013**, *46*, 60.

56. Han, S.; Chung, D. D. L. *Compos. Sci. Technol.* **2011**, *71*, 1944.

57. Liang, J.; Saha, M. C.; Altan, M. C. *Procedia Eng.* **2013**, *56*, 814.

58. Wang, S.; Haldane, D.; Gallagher, P.; Liu, T.; Liang, R.; Koo, J. H. *Compos. B: Eng.* **2014**, *61*, 172.